Journal of Chemistry and Technologies

THERMODYNAMIC ANALYSIS OF THE CLAUDE CYCLE FOR HYDROGEN LIQUIFICATION

Mykhailo. B. Kravchenko

Odesa National University of Technology. Kanatnaya Street, 112, Odesa, 65039, Ukraine

Abstract

Thermodynamic methods for reducing energy consumption are the most universal and practical. Therefore, the development of new thermodynamic analysis methods is relevant in the world preparing for the transition to the use of only renewable energy sources. This paper presents a new type of diagram that clearly shows the thermodynamic losses in the apparatuses of cryogenic units. The use of the Q–1/T diagram for the thermodynamic analysis of low-temperature cycles is illustrated on the basis of specific examples. Based on the given thermodynamic analysis, the areas of improvement of the hydrogen Claude cycle are identified for future hydrogen liquefaction plants with optimized energy efficiency. This work focuses on the application of new methods and innovative concepts, which are readily available. They will allow their implementation in hydrogen liquefaction plants in the near future.

Keywords: Clean energy; hydrogen; liquefier; refrigeration; thermodynamic losses; entropy.

ТЕРМОДИНАМІЧНИЙ АНАЛІЗ ЦИКЛУ КЛОДА ДЛЯ ЗРІДЖЕННЯ ВОДНЮ

Михайло. Б. Кравченко

Одеський національний технологічний університет. Вулиця Канатна, 112, Одеса, 65039, Україна

Анотація

Використання термодинамічного аналізу з метою зменшення витрат енергії є найбільш універсальним і практичним методом. Тому поширення нових методів термодинамічного аналізу є актуальною у світі, який готується до переходу на використання лише відновлюваних джерел енергії. У цій роботі представлено новий вид діаграми, які дозволяють наочно продемонструвати термодинамічні втрати в апаратах кріогенних установок. На конкретних прикладах проілюстровано особливості застосування діаграми Q-1/T для термодинамічного аналізу низькотемпературних циклів. На основі проведеного термодинамічного аналізу визначено принципи побудови водневих циклів Клода для перспективних установок зрідження водню з оптимізованою енергоефективністю. Ця стаття зосереджена на застосуванні нових методів та інноваційних концепцій, які є легкими у використанні. Тому ці методи можна використовувати для покращення майбутніх кріогенних установок для зрідження газів.

Ключові слова: чиста енергія; водень; зріджувач; охолодження; термодинамічні втрати; ентропія.

Introduction

Renewable energy sources have relatively low specific power. For this reason, renewable energy production cannot be concentrated in one place. Such distributed renewable energy production requires the creation of an infrastructure to store this energy, for example in the form of liquid hydrogen. This allows it to be transported over long distances and stored for long periods of time [1–3]. Therefore, the development of new schemes of low and medium capacity hydrogen liquefiers that can store hydrogen for later distribution is highly relevant.

Liquid hydrogen was first produced by J. Dewar in 1898. He used the Jowl-Tomson method with pre-cooling with liquid air to liquefy hydrogen. This method of liquefaction is so simple and effective that it is still widely used in small capacity liquefiers [4; 5]. There are several modifications of this method. However, they are all significantly less efficient than hydrogen liquefaction cycles using expanding turbines [6–10].

The first large-scale hydrogen liquefaction plants were built in 1960 to support the Apollo program. As of 2009, there are 10 hydrogen liquefaction plants in the U.S. producing 6–35 tons per day (TPD), 4 plants in Europe producing 5–10 TPD, and 11 plants in Asia producing 0.3–11.3 TPD [6].

According to the 2020 data, the production of liquid hydrogen in the USA will be 241 tons per day, in Canada – 51 tons per day, in Europe – 20 tons per day and in Japan – 31 tons per day. There are plans to increase the production of liquid hydrogen in the USA by 90 tons per day; in Europe and Japan by 5.3 tons per day in the next years [11].

Hydrogen liquefiers in operation today can be categorized by type of refrigeration cycle into the reverse helium Brayton cycle and the hydrogen Claude cycle. The helium Brayton cycle is typically used for smaller liquefiers with a capacity of 3 TPD or less. This is due to the lower capital costs associated with standardized helium expansion engines and screw compressors [12].
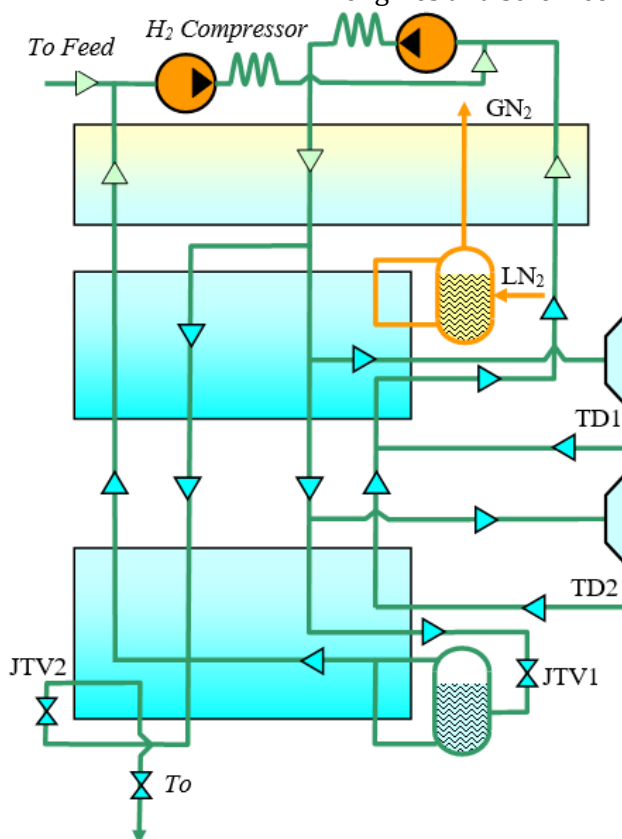
Fig. 1. Praxair hydrogen liquefaction process (adapted from [14])

Larger liquefiers, up to 5 TPD or more, are typically designed with a hydrogen Claude cycle. These are characterized by more expensive reciprocating compressors, but higher energy efficiency and lower refrigerant costs [13].

Liquid nitrogen evaporation at 80 K is generally used for pre-cooling in both configurations [4–10].

Praxair currently has five hydrogen liquefaction plants in the U.S. with production ranging from 18 to 30 TPD of liquid hydrogen. The typical specific power consumption of these plants

is between 12.5 and 15 kWh per kilogram of liquid hydrogen [14; 15].

Figure 1 shows a Praxair hydrogen liquefaction process flow sheet [14]. It looks like the pre-cooled Claude cycle, but is more complicated for the large plant.

There are three heat exchangers in this system. The first is cooled using superheated nitrogen vapor and an external cooling system. The second is cooled by boiling liquid nitrogen and some pressure recycled hydrogen. The third heat exchanger is cooled by hydrogen expanding through two parallel expansion turbines and the Joule-Thomson valve. This process involves continuous ortho-para conversion below 80 K. Only the liquefied portion of the compressed hydrogen passes through the ortho-para conversion.

Another example of a modified pre-cooled Claude cycle in use today is the hydrogen liquefaction plant in Leuna, Germany, which began operations in 2007. This plant has a capacity of 5 TPD. A process flow diagram of the Leuna liquefier is shown in Figure 2.
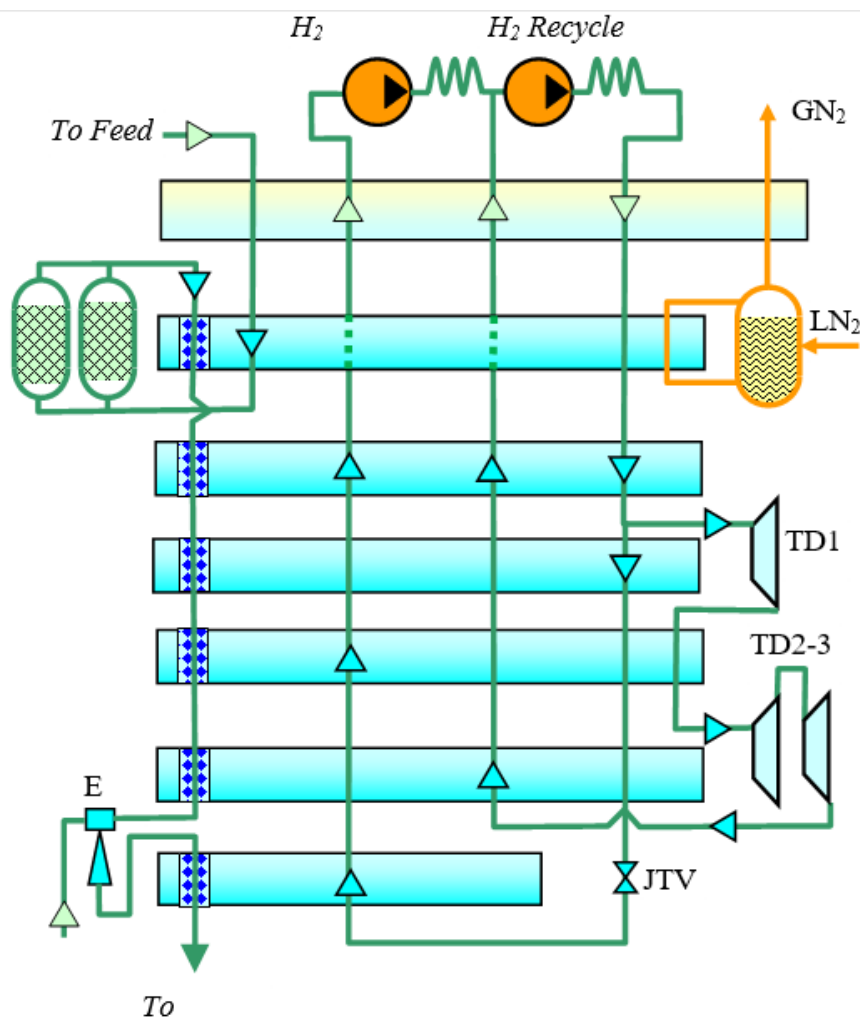
Fig. 2. Process flow sheet of hydrogen liquefaction plant in Leuna [15]

This plant also uses liquid nitrogen for cooling to 80 K and an improved hydrogen Claude process for cooling to 30 K. Three turbines in series at speeds up to 102,000 rpm with improved efficiency have been successfully tested in this plant [15].

The total specific liquefaction energy requirement is about 11.9 kWh/kg of liquid hydrogen [15]. The Leuna plant has a completely separate refrigeration cycle with normal hydrogen and receives a single feed hydrogen stream; there is no recycled hydrogen. The ortho-para conversions of the feed hydrogen are placed in heat exchangers.

All currently operating hydrogen liquefiers using Claude's hydrogen refrigeration cycle have some standard essential features:

✓ all hydrogen liquefiers use liquid nitrogen to pre-cool the feed and recirculating hydrogen streams;

✓ hydrogen is withdrawn to the first expander after the high pressure stream is cooled with liquid nitrogen;

✓ the final cooling of the process stream occurs from the circulating hydrogen boiling at near atmospheric pressure;

✓ the liquid hydrogen is formed after expansion in the JT valve.

It will be shown below that some of these essential features need to be corrected.

Construction and characteristic of Q–1/T diagrams.

Due to the higher prices of renewable energy, increasing the share of such energy requires a more economical use of this energy. Thermodynamic methods for reducing energy consumption are the most universal and practical. Therefore, the development of new thermodynamic analysis methods is relevant to the use of renewable energy sources.

Graphical representation of data is the most natural and convenient for humans, as we receive most of the information about the world around us visually. Computers "think" in large arrays of numbers that are difficult for humans to understand. Therefore, the language of graphical images is best suited for transferring information from a computer to a human. Thus, various types of diagrams and graphs will be used in scientific research and engineering practice in the foreseeable future.

The use of the Q–T diagram to define the behavior of heat exchangers is well known and widely used in the pinch analysis of heat exchangers. The Q–1/T diagrams used in this paper are similar to the Q-T diagrams and differ from them only in that this diagram is compressed by a factor of 1/T in the temperature range above 1K [16; 17].

Each line on the Q-T diagram corresponds to a line on the Q-1/T diagram. Furthermore, if the lines on the Q-T diagram intersect, then the corresponding lines on the Q-1/T diagram will also intersect. Consequently, the Q-1/T diagram retains the basic properties of Q-T diagrams, namely, it allows us to estimate the possibility and efficiency of heat transfer between heat transfer fluids.

The Q–1/T diagram also shows the thermodynamic losses associated with transferring heat at finite temperature differences, such as in heat exchangers.

The formula for defining the increase in entropy during the transfer of dq joules of heat from a flow with a temperature T_H to a flow with a temperature T_C is:

$$dS = dq \cdot \left[\frac{1}{T_C} - \frac{1}{T_H} \right]. \tag{1}$$

It is easy to verify that the right side of this equation is an elementary area equal to the area enclosed between the lines of hot and cold flows on the Q–1/T diagram. Consequently, the total increase in entropy in the heat exchanger is equal to the area of the 1/T diagram enclosed between the lines of the hot and cold flows:

$$\Delta S = \int_{q1}^{q2} \frac{1}{T_C(q)} dq - \int_{q1}^{q2} \frac{1}{T_H(q)} dq = \int_{q1}^{q2} \left[\frac{1}{T_C(q)} - \frac{1}{T_H(q)} \right] dq \tag{2}$$

where T_H and T_C are the temperatures of the warm and cold streams, respectively.

According to the Gouy-Stodola theorem, thermodynamic losses (exergy losses) can be found as

the product of the entropy increment and the ambient temperature. Therefore, up to a constant factor equal to the ambient temperature, the area enclosed by the heat and cold flow curves is equal to the thermodynamic losses in the heat exchanger.

The Q-1/T diagram must show not only the absolute value of the thermodynamic losses, but also clearly indicate the parts of the heat exchanger where the most significant entropy increase occurs.

At present, the heat exchanger efficiency is widely used to evaluate the quality of heat exchangers. By definition, the heat exchanger efficiency is defined as the ratio of the heat transferred in the actual heat exchanger to the heat that would be transferred in the ideal heat exchanger, i.e. the heat exchanger with infinite heat exchange surface. This quantitative indicator is very convenient for calculating the heat exchange area using the number of heat transfer units. However, the efficiency of a heat exchanger does not take into account the quality of the heat transferred or, which is the same thing, the temperature level at which the heat transfer takes place.

For the thermodynamic analysis of heat exchangers, it is advisable to use the exergy efficiency as a Figure of Merit (FOM) [18], which, for heat exchangers operating at temperatures below ambient temperature, is the ratio of the exergy increase of the hot flow to the exergy decrease of the cold flow.

The "heat capacity rate of the fluid of interest" is defined here as the product of the mass flow rate and the specific heat of the fluid of interest.

In the general case, when the heat capacity rates of the flows change in the course of heat

$$FOM = \frac{\int\limits_0^Q \left(\frac{1}{T_H(q)} - \frac{1}{T_E} \right) dq}{\int\limits_0^Q \left(\frac{1}{T_C(q)} - \frac{1}{T_E} \right) dq},$$ (3)

where T_H is the current temperature of the warm stream; T_C is the current temperature of the cold stream; T_E is the ambient temperature; dq is the elementary amount of heat transferred in the heat exchanger; Q is the heat load of the heat exchanger.

For the thermodynamic analysis of cryogenic cycles, it is crucial that the FOM of heat exchangers does not become 100 % even with an infinite heat exchange surface [18]. The only exception is

exchange, for heat exchangers operating at temperatures below ambient, the formula for determining the FOM of the heat exchanger takes the form:

counterflow heat exchangers with equal heat capacity rates of cold and heat flows.

Consider the Q–1/T diagram of the heat exchanger of a Joule-Thomson cryocooler operating on nitrogen, see Figure 3. The pressure of the hot stream is assumed to be 200 bar. The temperature of the cold stream at the hot end of the heat exchanger is assumed to be 290 K, and the initial temperature of the hot stream is assumed to be 300 K.
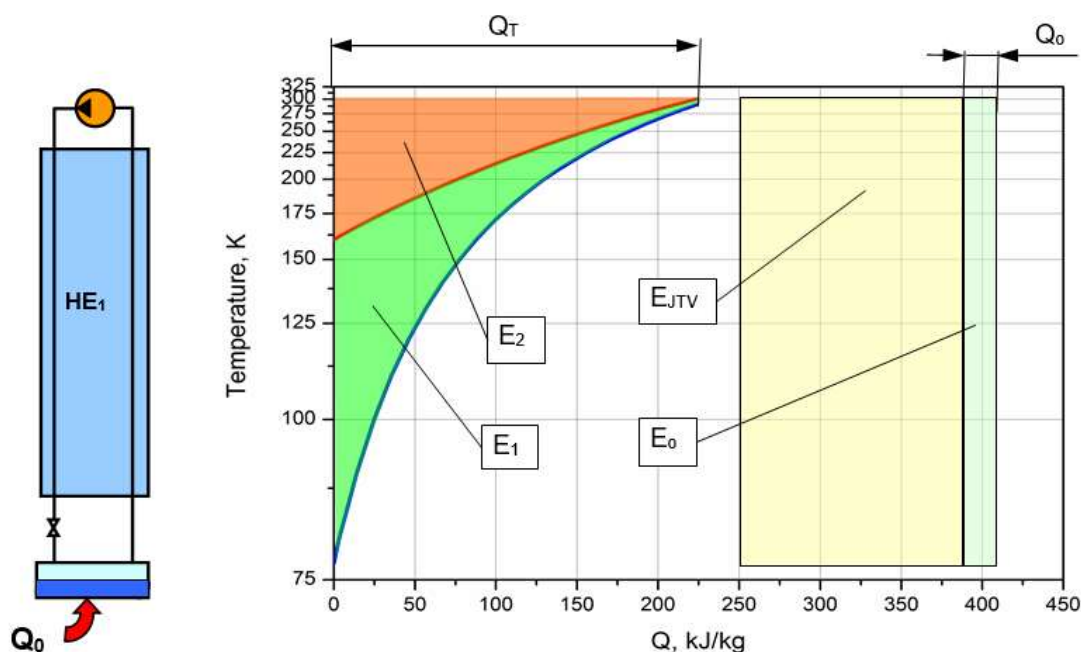
Fig. 3. Q–1/T diagram of the Joule-Thomson cycle cryocooler.
E_1 – thermodynamic losses in the heat exchanger; E_2 – exergy of the hot flow; E_{JTV} – thermodynamic losses in the throttle valve; E_0 – the exergy of the heat removed in the evaporator; Q_0 – cooling capacity of the cryocooler; Q_T – heat load of heat exchanger

In the diagram, the blue line corresponds to the cold stream and the red line corresponds to the hot stream. The area of figure E_1 is proportional to the exergy of the hot stream. The area of figure E_2 is proportional to the thermodynamic losses in the heat exchanger. The exergy of the cold stream is proportional to the sum of the areas of figures E_1 and E_2. It follows that the *FOM* of the heat exchanger can be found as the ratio of the area of figure E_1 to the sum of the areas of figures E_1 and E_2:

$$FOM = \frac{S_{E1}}{S_{E1} + S_{E2}} \cdot 100\%$$ (4)

The calculation shows that the maximum *FOM* of the heat exchanger in the considered Joule-Thomson cycle is 48 %. In other words, in the heat exchanger of the considered cryocooler operating in the Joule-Thomson cycle, more than 50 % of the cold flow exergy is lost [18].

In addition to heat exchangers, cryocoolers include other elements - Joule-Thomson or JT valves, expanders, evaporators, mixers, etc.

Let's consider how to represent thermodynamic losses in these low-temperature elements on the Q–1/T diagram.

The exergy of the heat removed in a low-temperature evaporator can be found from the formula:

$$E_0 = Q_0 \cdot \left[\frac{T_E - T_0}{T_0} \right] = Q_0 \cdot \left[\frac{1}{T_0} - \frac{1}{T_E} \right] \cdot T_E, \quad (5)$$

where T_0 is evaporation temperature; Q_0 is heat removed in the evaporator.

Consequently, on the Q–1/T diagram, the exergy of heat of vaporization will be similar to the area of a rectangle of width Q_0 enclosed between the isotherms T_E and T_0.

It is not difficult to find the entropy increase during gas expansion in the JT valve. Therefore, the thermodynamic losses in the throttle are conveniently represented as a rectangle enclosed by the isotherms T_E and T_0. The width of this rectangle can be found using the formula:

$$q_{JTV} = \frac{\Delta s_{JTV}}{\left[\frac{1}{T_0} - \frac{1}{T_E} \right]}, \quad (6)$$

where ΔS_{JTV} is the entropy increment in the JT valve.

It makes it possible to plot figures on the Q–1/T diagram whose areas are proportional to the exergy of the heat removed from the object to be cooled, the losses of exergy in the heat exchanger and the JT valve.

For the considered Joule-Thomson cryocooler, the exergy of the compressed gas entering the heat exchanger is equal to the sum of the thermodynamic losses in the installation elements plus the exergy of the heat removed in the evaporator:

$$E = T_E \cdot \sum_{i=1}^{n} \Delta S_i + Q_0 \cdot \left[\frac{1}{T_0} - \frac{1}{T_E} \right] \cdot T_E. \quad (7)$$

Therefore, if the gas parameters at the compressor inlet and outlet do not change, the sum of the areas of all parts of the Q–1/T diagram remains constant. This is a fascinating and essential property of Q–1/T diagrams, since neither the exergy of individual flows nor the refrigeration capacity has this property.

The constancy of the Q–1/T diagram area makes the thermodynamic analysis of low temperature systems more intuitive. In some cases, it allows us to simplify the study itself. For example, when part of the hot flow expands in the expansion engine, the area of the section corresponding to the losses in the JT valve decreases by the amount of the expansion work, see Figure 4.
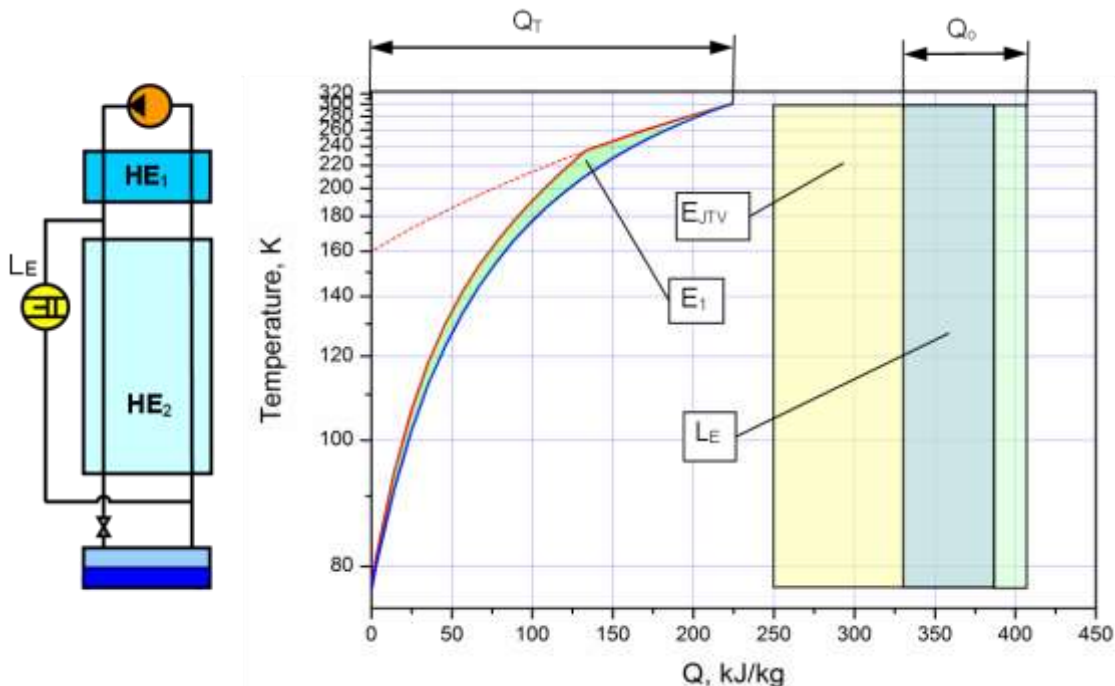
Fig. 4. Q-1/T diagram of the cryocooler operating on the Cloud cycle.
E_1 – thermodynamic losses in the heat exchanger; L_E – mechanical work of the expander; E_{JTV} – thermodynamic losses in the JT-valve; Q_0 – cooling capacity of the cryocooler; Q_T – heat load of the heat exchanger

The area of the section corresponding to the exergy of the heat removed in the evaporator will increase by the expander work.

Thus, the boundary of the sections of the diagram corresponding to the JT valve losses and the exergy of the heat removed in the evaporator will move by the value of the expander work.

It is desirable to maximize the fraction of gas entering the expander and reduce the fraction of gas expanding in the JT valve to reduce thermodynamic losses and increase the efficiency of the cryogenic cycle. However, there are limits to increasing the proportion of expander gas flow.

As some of the gas is drawn into the expander, the heat capacity rate of the hot stream decreases. As a result, the temperature difference between the hot and cold gas streams begins to decrease after some of the gas is drawn into the expander. The minimum temperature difference between the gas streams in the heat exchangers limits the maximum fraction of gas that can be directed to the expander motor. Therefore, gas should be drawn into the expander where the temperature difference between the hot and cold gas streams is maximum. The maximum temperature difference between the hot and cold gas streams allows us to achieve the maximum gas flow rate into the expander.

Another conclusion that can be drawn from the thermodynamic analysis is that the losses in the JT valve decrease with decreasing gas temperature upstream of this valve. Therefore, to increase the efficiency of thermodynamic cycles, it is desirable to reduce the gas temperature as much as possible before throttling. This conclusion is far from obvious because reducing the temperature upstream of the JT valve reduces the temperature difference between the inlet and outlet of the JT valve and reduces the Joule-Thomson effect in the throttle valve.

By calculating the entropy increment on the Q–1/T diagram, it is easy to show the losses due to the mixing of working materials of different temperatures or compositions.

It is easy to determine the amount of heat that can be removed from a warm stream if the minimum temperature at which this heat is removed is known, see Figure 5.

To do this, simply draw an isotherm on the Q–1/T diagram corresponding to this minimum temperature of heat removal. The length of the segment between the intersection points of this isotherm with the hot and cold stream lines will correspond to the maximum amount of heat that can be removed from the hot stream. The area of the rectangle built on this segment and the isotherm of the environment will be proportional to the exergy of the heat removed. The diagram clearly shows that the amount of heat removed from the hot stream decreases rapidly as the heat removal temperature approaches the ambient temperature.
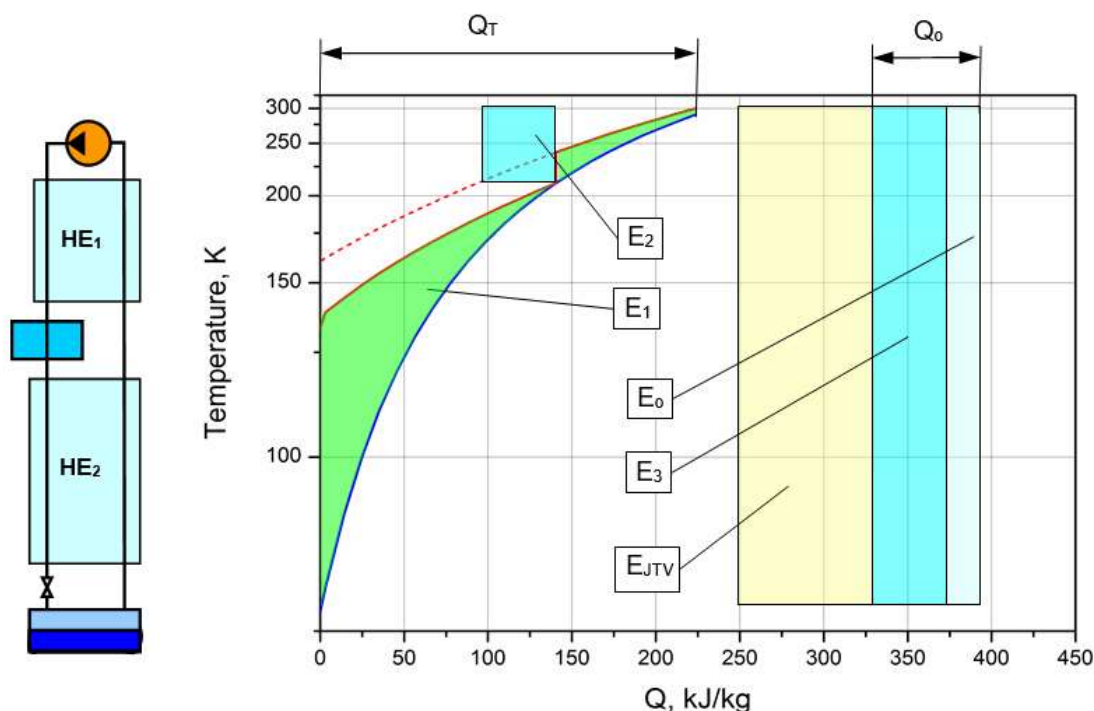
Fig. 5. Q–1/T diagram of a Joule-Thomson cycle nitrogen cryocooler with intercooling.
E_1 – thermodynamic losses in the heat exchanger; E_2 – exergy of heat removed from the warm flow;
E_3 – exergy of heat on which to increase the cooling capacity of the cryocooler; E_0 – exergy of the heat removed from the object to be cooled without intercooling; E_{JTV} – thermodynamic losses in the throttle

It is easy to show a decrease in imperfect heat transfer losses when heat is removed from a warm stream. The reduction of thermodynamic losses is proportional to the area of the figure enclosed between the line of the warm stream without heat removal and the line of the warm stream with heat r emoval.

It is well known that heat removal during pre-cooling of a warm stream leads to an increase in the cooling capacity of low-temperature units by exactly the amount of heat removed. However, the exergy of the heat removed at the pre-cooling temperature is less than the exergy of the same amount of heat added in the evaporator. This "nonequivalent exchange" can be easily explained using the Q–1/T diagram.

This "nonequivalent exchange" is due to the reduction of thermodynamic losses in the heat exchanger and the JT valve. The reduction of the exergy losses in the heat exchanger and the throttle valve, plus the exergy of the heat removed from the hot stream, is equal to the increase of the exergy of the heat transferred in the evaporator. It follows that in order to increase the efficiency of the cryogenic cycle, the maximum amount of heat should be removed at each intermediate temperature.

Compare the Q–1/T diagrams of cryocoolers with the expansion of the gas flow fraction and the cooling of the hot flow. It can be concluded that cooling the hot stream before it is drawn into the expander will result in a decrease in the expander stream fraction compared to its fraction without pre-cooling. Therefore, pre-cooling the gas before it is drawn into the expander will reduce the effect of the expander.

When using Q–1/T diagrams to analyze cryogenic plants operating at helium and hydrogen temperatures, the shape of the diagrams is too compressed at high temperatures. This causes certain inconveniences in the use of Q–1/T plots.

Figure 6a shows the Q–1/T diagram for a hydrogen Joule-Thomson cryorefrigerator with liquid nitrogen precooling. The pressure of the hot hydrogen stream is assumed to be 12 MPa.

In this diagram, the lines of the hot and cold flows practically merge in the temperature range
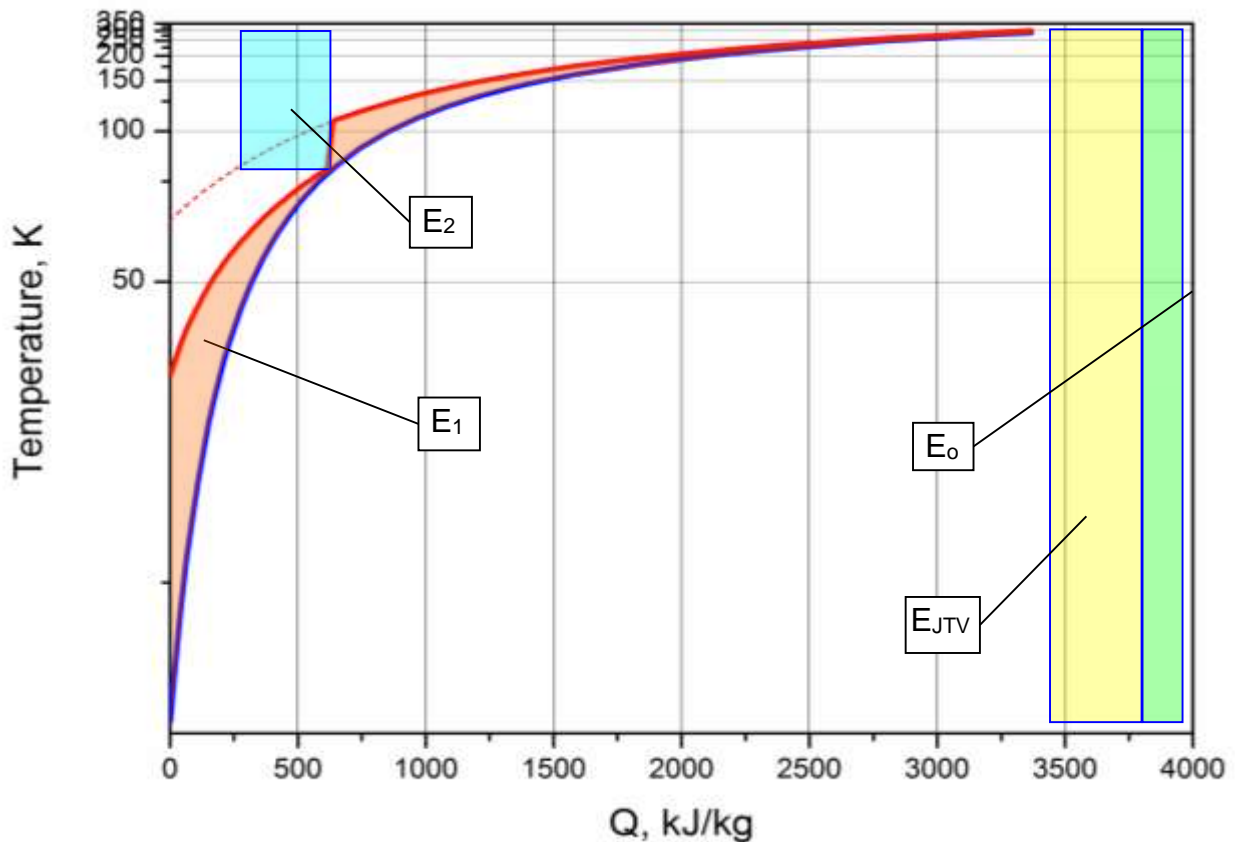
Fig. 6a. Q–1/T diagram of a Joule-Thomson cycle hydrogen cryorefrygarator with liquid nitrogen intercooling.
E_1 – thermodynamic losses in the heat exchanger; E_2 – exergy of heat removed from the warm flow;
E_0 – exergy of the heat removed from the object to be cooled; E_{JTV} – thermodynamic losses in the JT-valve

above 200 K. This indicates that in this temperature range the temperature difference has a small effect on the total thermodynamic losses in the cycle. On the other hand, this causes inconvenience when working with the Q–1/T diagram, because the diagram is poorly detailed in this temperature range. We can divide the Q-1/T diagram into several parts with different scales along the abscissa and ordinate axes to eliminate these inconveniences.

In order to maintain the clarity of the Q-1/T diagram, it is essential that after changing the scale of its axes, the areas of the figures on the diagram remain unchanged. This is achieved by simultaneously decreasing the scale of the heat quantity axis and increasing the scale of the temperature axis by the same amount.

Really:

$$\Delta S = \int_{q_1}^{q_2} \left[\frac{1}{T_C} - \frac{1}{T_H} \right] \cdot dq = \int_{q_1}^{q_2} \left[k \cdot \left(\frac{1}{T_C} \right) - k \cdot \left(\frac{1}{T_H} \right) \right] \cdot d\left(\frac{1}{k} q \right). \tag{8}$$

The shape and size of the figures on the Q-1/T diagram change with a change in the axis scale, but their areas remain unchanged. It makes it possible to compare the thermodynamic losses in the Q–

1/T sections of the diagram with different axis scales.

Figure 6b shows the Q–1/T view of the diagram for the heat exchangers of a cryocooler operating

Fig. 6b. Q–1/T diagram of a Joule-Thomson cycle hydrogen cryorefrygarator with liquid nitrogen intercooling, divided into two parts according to the 80 K isotherm.
E₁ – thermodynamic losses in the heat exchanger located before the liquid nitrogen bath;
E₂ – exergy of heat removed from the liquid nitrogen bath;
E₃ – thermodynamic losses in the heat exchanger located under the liquid nitrogen bath

on the Joule-Thomson cycle on hydrogen, divided into two parts according to the 80 K isotherm. The heat load scale for the heat exchangers located in front of the nitrogen bath is reduced by three times in comparison with the heat load scale for the heat exchangers located under the nitrogen bath. At the same time, the scale of the temperature axis has been increased by three times.

It can be seen that the thermodynamic losses in the heat exchangers of the cryocooler below and above the nitrogen level of temperature are comparable. This is despite the fact that the heat load of the heat exchanger located below the nitrogen bath is about six times lower than the heat load of the heat exchanger located above the nitrogen bath.

The use of Q–1/T diagrams in the cryogenic temperature range is particularly evident because the lower the temperature, the more the shape of the curves on the Q–1/T diagrams differs from the shape of the corresponding curves on the regular Q–T diagrams.

Advanced Claude's hydrogen liquefaction cycle

Figure 7 shows the flow diagram of the proposed hydrogen liquefier that implements the recommendations based on the thermodynamic analysis.

The thermodynamic analysis carried out on elementary cryogenic cycles allows to formulate several recommendations that should be followed when designing effective cycles of cryocoolers and gas liquefaction units.

Before applying these principles to the construction of a new cycle, we list them once again:

✓ when designing cryogenic refrigeration circuits, it is necessary to remove as much heat as possible by means of an external refrigerant. Removing heat at an intermediate temperature level allows us to supply the same amount of heat at the lowest temperature level;

✓ withdrawing some of the working fluid to the expander should be done before an external refrigerant cools the compressed gas stream, allowing an increase in the proportion of gas that expands in the expander;

✓ prior to expansion in the JT valve, the gas temperature must be reduced as much as possible. This reduces the thermodynamic losses in the throttle valve;

✓ the heat capacity rates of the hot and cold flows in heat exchangers should be as close to each other as possible; this makes it possible to reduce

Fig. 7. Proposed flow diagram of a hydrogen liquefier operating on the modified Claude's cycle

the irreversibility of heat transfer at a finite temperature difference.

The hydrogen feed stream is completely separated from the circulating hydrogen in the Claude's cycle and enters the unit at a supercritical pressure of 2.4 MPa. This eliminates condensation of liquid hydrogen in the channels of the heat exchangers and improves the conditions for heat exchange with the circulating hydrogen stream. The pressure of the feed hydrogen makes it possible to liquefy the hydrogen obtained by hydrolysis of water without additional compression [19]. This is because it is possible to obtain sufficiently pure hydrogen from water hydrolysis at pressures of up to 3 MPa.

The circulating hydrogen flow forms the Claude cycle with three expanders connected in series. The series connection of the expanders ensures the maximum gas flow in each of the expanders with the minimum expansion ratio in them. Such an expander connection scheme also allows the use of turbomachines with high adiabatic efficiency. The circulating hydrogen pressure at the compressor outlet is assumed to be 2.5 MPa. It will allow efficient use of reciprocating compressors for compression of circulating hydrogen flow and turboexpanders for its expansion.

The first feature of the proposed hydrogen liquefaction scheme is that the hydrogen feed stream is cooled to 80 K only by the evaporation of liquid nitrogen and the heating of the formed vapors to a temperature close to the ambient temperature. In this case, the hot hydrogen flow leaving the compressor is cooled only by the counterflow of circulating hydrogen at low pressure. It allows to obtain the maximum temperature difference between the hot and cold streams of circulating hydrogen at its outlet to the first expander.

The temperature of the hydrogen taken into the first expander was assumed to be 97.8 K. The temperature difference between the hot and cold streams of the circulating hydrogen at this point is 24.4 K, which allows 90.5 % of the hydrogen to be taken for expansion in the expander. The remainder of the high-pressure recirculating stream (9.5 %) is cooled to 80 K in a bath of liquid nitrogen.

Figures 8a-d show Q–1/T diagrams for the heat exchangers of the plant, constructed so that the areas of the figures enclosed between the curves of the hot and cold flows are proportional to the thermodynamic losses during heat transfer. Figure 8a shows the form of Q–1/T diagrams for the HE1 heat exchanger.
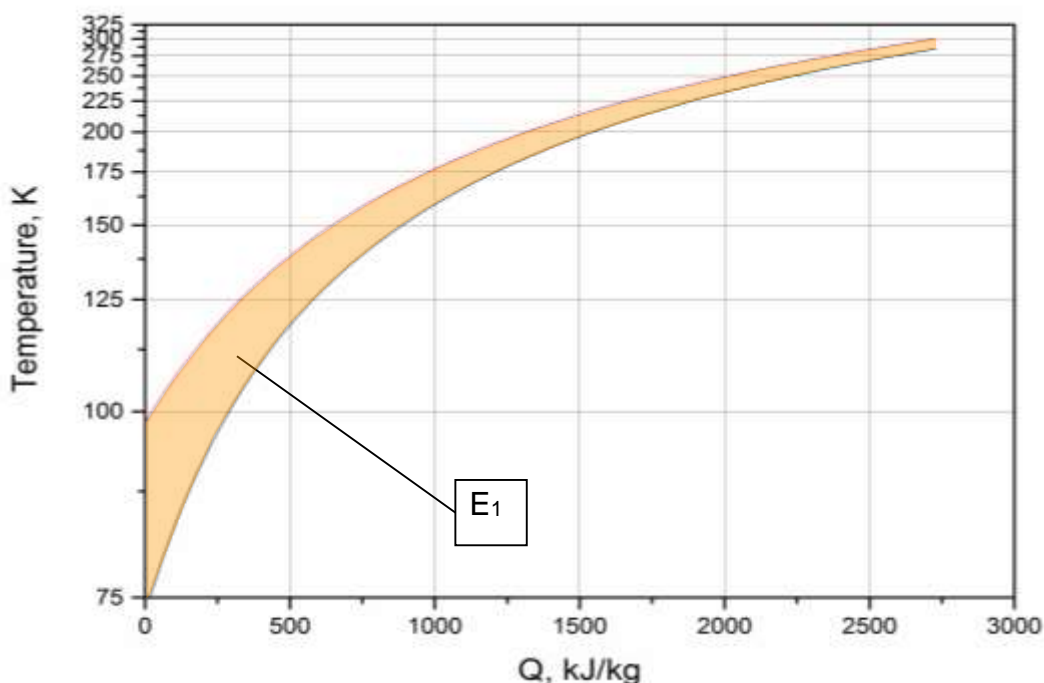
Fig. 8a. The Q-1/T diagrams for the HE1 heat exchanger of the proposed hydrogen liquefier operating on the modified Claude cycle.
E_1 – thermodynamic losses in HE1 heat exchanger
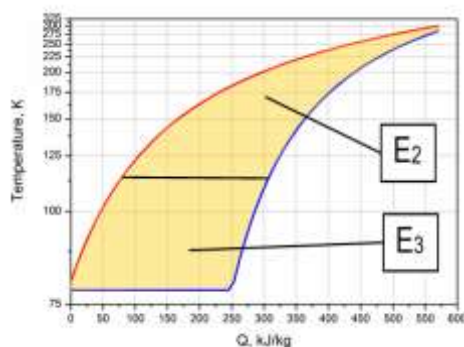
Fig. 8b. The Q–1/T diagrams for the HE2 heat exchanger and the liquid nitrogen bath (LNB) of the proposed hydrogen liquefier operating on the modified Claude cycle.
E_2 – thermodynamic losses in HE2 heat exchanger that can be compensated by LNG boiling; E_3 – thermodynamic losses in HE2 heat exchanger and LNB that can be compensated by liquid nitrogen boiling

Figure 8b shows a Q–1/T diagram of HE2 heat exchanger and liquid nitrogen bath (LNB). A comparison of these diagrams shows that the thermodynamic losses in the HE2 heat exchanger and liquid nitrogen bath are higher than those in the HE1 heat exchanger. The separate arrangement of the HE2 heat exchanger and the liquid nitrogen bath allows these losses to be compensated for by evaporating the liquid nitrogen rather than reducing the usable liquid hydrogen capacity of the plant.

The consumption of liquid nitrogen can be reduced by using an external refrigeration unit to remove part of the heat at an intermediate temperature level.

The first turboexpander's adiabatic efficiency is taken equal to 0.85; the hydrogen pressure at the outlet of the first turboexpander is 0.83 MPa; the expansion ratio in the first expander is 3.0. The temperature of the hydrogen leaving the first expander is 68.2 K.

In Figure 8c is a Q–1/T diagram showing the composite curve (red line) of three warm streams - the hydrogen procession stream, the high pressure (2.5 MPa) circulating stream, and the circulating stream exiting the 1st expander [15]. The blue line in this diagram shows the composite curve of the cold stream, including the hydrogen stream exiting the last expander (0.15 MPa) and the throttle hydrogen stream at 0.11 MPa.

The junctions in the hot stream curve correspond to the entry and exit points of the hydrogen expander stream. At the entry point of the hydrogen stream leaving the first expander, the temperature difference is 1.8 K. The expansion of the hydrogen in the first expander to a lower pressure is not possible because it would lead to the intersection of the lines of the hot and cold streams.

After the return of the hydrogen stream expanded in the first expander, the temperature difference between the combined hot and cold streams begins to increase and reaches 7.7 K. At this point, with a temperature of 55 K, the expander stream enters the turboexpander series of connected 2nd and 3rd expanders. The rate of hydrogen expansion in these expanders is 2.4; therefore, the adiabatic efficiency of these expanders is assumed to be 0.87. The temperature of the hydrogen leaving these expanders is 30.7 K.

At a pressure of 2.4 MPa and a temperature of about 40 K, the supplied hydrogen stream has a maximum heat capacity, reflected in the Q–1/T diagram as a local decrease in temperature difference near 40 K.

The expansion of hydrogen in turboexpanders from a temperature of 55 K to a temperature of 30.7 K provides cooling of two warm high pressure hydrogen streams to a temperature of 32.5 K. This is the minimum temperature to which it is possible to cool circulating hydrogen before the JT valve. When the hydrogen is throttled to a pressure of 0.11 MPa, 62 % liquid hydrogen is produced. This hydrogen boils at 20.7 K.

This hydrogen is used to cool the processed hydrogen stream to a temperature below 21.0 K. A liquid hydrogen single phase wet expander is used to reduce the pressure of the processed hydrogen from supercritical to storage pressure of 1 bar. Liquid hydrogen expanders have a high adiabatic efficiency of more than 90 % [5; 13; 20]. Liquid hydrogen at atmospheric pressure is produced at the expander outlet.

In order to obtain hydrogen that can be stored in liquid form for a long period of time, it is necessary to carry out an ortho-para conversion to this hydrogen [21]. The ortho-para conversion of hydrogen is accompanied by the release of a large amount of heat. Therefore, it is desirable to carry out the ortho-para conversion at the highest possible temperature. The first stage of ortho-para conversion takes place at the liquid nitrogen

temperature level. It is advisable to install the ortho-para conversion catalyst in a liquid nitrogen bath, since the cooling of the hydrogen feed stream to a temperature of 80 K is performed with liquid nitrogen. In this case, the heat of ortho-para conversion is removed by boiling the liquid nitrogen. The equilibrium concentration of parahydrogen at a temperature of 80 K is about 48 %. Therefore, in the calculations, the parahydrogen concentration in the treated stream after the liquid nitrogen bath was assumed to be 45 %.
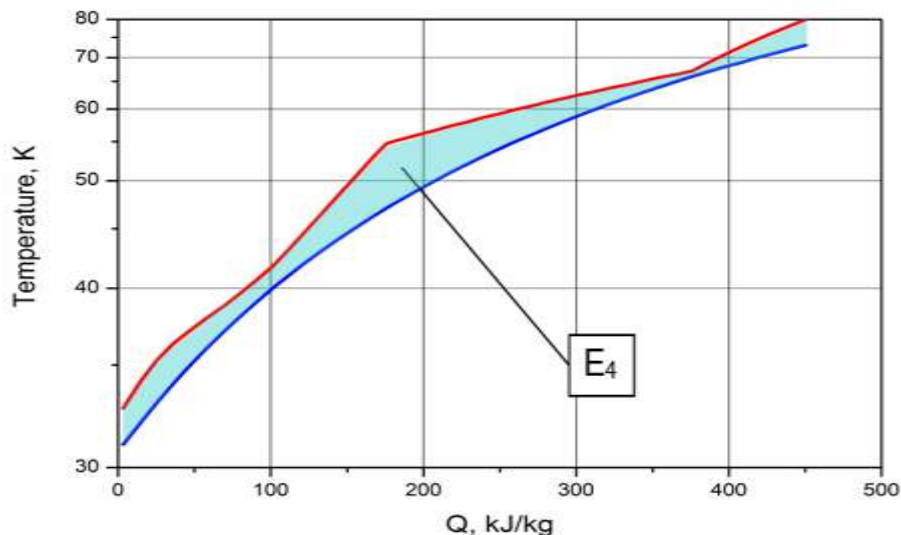
Fig. 8c. Composite Q–1/T diagrams for the HE3 and HE4 heat exchangers of the proposed hydrogen liquefier. E$_4$ – thermodynamic losses in HE3 and HE4 heat exchanger
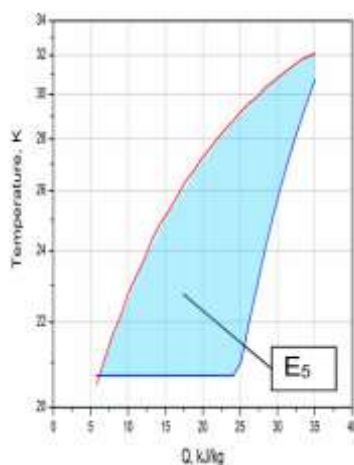
Fig. 8d. Composite Q–1/T diagrams for the HE5 heat exchanger and liquid hydrogen bath LHB of the proposed liquefier of hydrogen. E$_5$ – thermodynamic losses in HE5 heat exchanger and liquid hydrogen bath LHB

In the temperature range from 80 K to 30 K, the ortho-para conversion should be performed continuously as the hydrogen product stream is cooled. It is assumed that the catalyst for ortho-para conversion is uniformly distributed in the channel for the processed flow in heat exchangers HE3 and HE4. This solution ensures the performance of the heat exchangers in this temperature range. Without ortho-para conversion, the composite curves of the hot and cold flows would intersect on the Q–1/T diagram, making heat transfer impossible at the selected flow parameters.

At the temperature of 30 K, the parahydrogen equilibrium concentration reaches 96.5 %; therefore, in the calculations, the parahydrogen concentration at the outlet of this heat exchanger is assumed to be 95 %. In the liquid hydrogen bath, where the final cooling of the treated hydrogen takes place before it is fed to the single-phase expander, an ortho-para conversion catalyst is placed. It is provided that the concentration of parahydrogen in the processed liquid hydrogen is brought to 99%.

The calculations showed that for hydrogen obtained by hydrolysis of water, the energy

consumption for liquefaction of 1 kg of 99% parahydrogen is 11.2 kWh. If liquefied natural gas is used to pre-cool the feed hydrogen, the energy consumption for liquefying 1 kg of 99% parahydrogen can be reduced to 7.5 kWh.

Results and discussion

Distributed generation of renewable energy will require the creation of an infrastructure for the accumulation of liquid hydrogen and its transportation over long distances. Therefore, the development of new schemes of low and medium capacity hydrogen liquefiers that can accumulate hydrogen for subsequent distribution is highly relevant.

Hydrogen liquefiers up to 5 TPD or higher are typically designed with a hydrogen Claude cycle. These feature higher energy efficiency and lower refrigerant costs. Therefore, the hydrogen Claude cycle requires all kinds of improvements to reduce the energy consumption.

The use of Q-1/T diagrams for the thermodynamic analysis of low-temperature cycles is illustrated with specific examples. Based on the given thermodynamic analysis, the areas for improvement of the hydrogen Claude cycle are identified for future hydrogen liquefaction plants with optimized energy efficiency.

Based on the given thermodynamic analysis, a new design of the Claude cycle hydrogen liquefier has been proposed.

Conclusions

The thermodynamic analysis carried out on elementary cryogenic cycles makes it possible to formulate several recommendations that should be applied to improve the hydrogen Claude cycle:

✓ it is necessary to remove as much heat as possible with an external refrigerant;

✓ some of the working fluid should be withdrawn to the expander before an external refrigerant cools the high-pressure gas stream;

✓ the gas temperature must be reduced as much as possible before expansion in the JT valve;

✓ the heat capacity rates of the hot and cold flows in heat exchangers should be as close to each other as possible.

The new scheme of the hydrogen liquefier was proposed, which implements these recommendations made on the basis of thermodynamic analysis of the simplest cryogenic cycles.

The calculations showed that for the proposed hydrogen liquefier the energy consumption for liquefaction of 1 kg of 99% parahydrogen is 11.2 kWh.

References

[1] Mazloomi, K., Gomes, C. (2012). Hydrogen as an energy carrier: Prospects and challenges. Renew. Sustain. *Energy Rev.* 16, 3024–3033.

[2] Staffell, I., Scamman, D., Velazquez Abad, A., Balcombe, P., Dodds, P. E., Ekins, P., Shah, N., Ward, K. R. (2019). The role of hydrogen and fuel cells in the global energy system. Review. *Energy Environ. Sci.*, 12, 463–491.

[3] Mikul, H. (2021). Energy transition and the role of system integration of the energy, water and environmental systems. *J. Clean. Prod.*, 292, 126027.

[4] Yin, L., Ju, Y. (2020). Review on the design and optimization of hydrogen liquefaction processes. *Front. Energy*, 14, 530–544.

[5] Zhang, T., Uratani, J., Huang Y., Xu L., Griffiths, S., Ding, Y. (2023). Hydrogen liquefaction and storage: Recent progress and perspectives. *Renewable and Sustainable Energy Reviews*, 176, 113204.
https://doi.org/10.1016/j.rser.2023.113204

[6] Krasaein, S., Stang, J. H., Neksa, P. (2010). Development of large-scale hydrogen liquefaction processes from 1898 to 2009. *Int. J. Hydrogen Energy*, 35, 4524–4533.

[7] Zou, A., Zeng, Y., Luo, E. (2023). New generation hydrogen liquefaction technology by transonic two-phase expander. *Energy, 272*, 127150.

[8] Aasadnia, M. Mehrpooya, M. (2018). Large-scale liquid hydrogen production methods and approaches: A review. *Applied Energy*, 212, 57–83. doi: 10.1016/j.apenergy.2017.12.033.

[9] Sadaghiani, Mirhadi S.; Mehrpooya, Mehdi (2017). Introducing and energy analysis of a novel cryogenic hydrogen liquefaction process configuration. International Journal of Hydrogen Energy, 42(9), 6033–6050.
doi: 10.1016/j.ijhydene.2017.01.136

[10] Zhang, S., Liu, G. (2022). Design and performance analysis of a hydrogen liquefaction process. *Clean Technologies and Environmental Policy*. 24, 51–65.

[11] Decker, L. (2020). Latest Global Trend in Liquid Hydrogen Production.
https://www.sintef.no/globalassets/project/hyper/presentations-day-1/day1_1430_decker_latest-global-trend-in-liquid-hydrogen-production_linde.pdf/.

[12] Chang, H. M., Ryu, K. N.; Baik, J. H. (2018), Thermodynamic design of hydrogen liquefaction systems with helium or neon Brayton refrigerator. *Cryogenics*, 91, 68–76.

[13] Al Ghafri, S. Z., Munro, S., Cardella, U., Funke, T., Notardonato, W., Trusler, M., Leachman, J., Span, R., Kamiya, Sh., Pearce, G., Swanger, A., Rodriguez, E. D., Bajada, P., Jiao, F., Peng, K., Siahvashi, A., Johns, M. L., May, E. F. (2022). Hydrogen liquefaction: a review of the fundamental physics, engineering practice and

future opportunities. (Review Article)*. Energy Environ. Sci., 15,* 2690–2731. doi: 10.1039/D2EE00099G

[14] Drnevich, R. (2003). Hydrogen delivery – liquefaction & compression. *Praxair, strategic initiatives for hydrogen delivery workshop – May 7, 2003.* https://www1.eere.energy.gov/hydrogenandfuel cells/pdfs/liquefaction_comp_pres_praxair.pdf

[15] IDEALHY – "Integrated Design for Efficient Advanced Liquefaction of Hydrogen". http://www.idealhy.eu/

[16] Kravchenko, M. B. (2004). Analysis of thermodynamic cycles of low temperature units using q-1/T diagrams. *Industrial gases.* 2, 43–46. (in Russian)

[17] Kravchenko, M. B. (2011). On the possibility of using a cryogenic cycle with a heat engine for liquefying natural gas. *Refrigeration Engineering and Technology.* 3 (131), 47–55. (in Russian)

[18] Razani, A., Dodson, C. Fraser, T. (2012). Exergy-based figure of merit for regenerative and recuperative heat exchangers with application to multistage cryocoolers. *Advances in Cryogenic Engineering AIP Conf. Proc., 1434*, 1830–1838. doi: 10.1063/1.4707120

[19] Maha, R., Marine, T., Florence, D., Jonathan, D., and Marian, C. (2020). Electrochemical hydrogen compression and purification versus competing technologies: Part II. Challenges in electrocatalysis. *Chinese Journal of Catalysis. 41*, 770–782

[20] Ohlig, K., Decker, L (2014). *The latest developments and outlook for hydrogen liquefaction technology.* Proc. of the 20th World Hydrogen Energy Conference Gwangju.

[21] Zhuzhgov, A. V., Krivoruchko, O. P., Isupova, L. A. Mart'yanov, O. N., Parmon, V. N. (2018). Low-Temperature Conversion of ortho-Hydrogen into Liquid para-Hydrogen: Process and Catalysts. Review. *Catalysis in Industry*. 10, 9–19. https://doi.org/10.1134/S2070050418010117